J. Fluid Mech. (1969), *vol.* 35, *part* 3, *pp.* 417–437
Printed in Great Britain

The temporal development of a model of high Rayleigh number convection

By J. W. ELDER

Department of Applied Mathematics and Theoretical Physics,
University of Cambridge

(Received 17 November 1967 and in revised form 10 August 1968)

The evolution of a model of the flow in a layer of fluid suddenly heated from below at a Rayleigh number sufficient for a laboratory flow to ultimately become turbulent is investigated with numerical experiments. The numerical study simulates the flow by means of the mean field equations along the lines of Herring's (1963, 1964) pioneering study but uses a different finite difference technique and concentrates attention on the flow *development* rather than on the final statistically steady state. These solutions are compared with previous and some new simulations in two dimensions. The solutions confirm Herring's work and in addition show that the mean field equations, and in particular the weak-coupling approximations, describe the gross features of the model sufficiently well for the mean field equations to be used with reasonable confidence in evolutionary studies.

1. Preliminary remarks

When a layer of fluid, initially at rest, is suddenly heated from below we observe after an interval of time the progressive development of convective motions till the whole layer is convecting. If the Rayleigh number is sufficiently high and sources of thermal noise are present the ultimate motion is unsteady, the whole field of flow having finite amplitude fluctuations of temperature and velocity. A number of laboratory experiments and some numerical simulations in two dimensions have been reported describing many of the detailed features of the motion but those studies make it difficult to obtain an overall description of the flow, in particular, of the evolution of the gross thermodynamic structure.

The information of greatest interest is contained in the mean field equations, where spatial means are taken over horizontal planes. A study of these equations is especially interesting because of the possibility of comparison with the recent two-dimensional simulation of the protosublayer (Elder 1968*a*). Our study is made possible by the work of Herring (1963, 1964) who in a pioneering numerical calculation of the mean field equations of the weak coupling approximation has

obtained results which agree broadly with the laboratory data. In many respects the results are surprisingly good in view of the harshness of the approximations, but here we accept the approach as a basis for further study. Although Herring's calculations involved the time development of the flow he was essentially interested in the ultimate statistically steady state. He does, however, give one figure (Herring 1963, p. 329, figure 1) showing the evolution of the Nusselt number. But these results do not necessarily give the correct temporal development. For example, in the study with rigid confining planes (Herring 1964) he places the Prandtl number $\sigma = \infty$ at the outset, since, as can be seen by inspection of the equations, in the final steady state the solution is independent of σ. Further he approximates the spatial spectra in the light of the symmetries of the final motion.

We will study the *time development* of Herring's model in some detail. In the course of the work we are also able to verify Herring's calculations, clarify a number of minor details, and simplify both the calculations and their interpretation. Now the essential feature of Herring's numerical method is the use of a truncated Fourier representation of the field variables. But some of his data, in particular the small bumps in the mean temperature on the margin of the sublayer (e.g. Herring 1963, p. 332, figure 7) which suggest a type of Gibbs-phenomena, indicate a possible weakness of the finite Fourier representation. In the iterative finite difference method used here this possible difficulty does not exist but we are able to essentially confirm Herring's results for the statistically steady state. Further, because in the statistically steady state the boundary conditions imply that the Fourier modes of odd parity are zero these modes are (legitimately) neglected in Herring's calculations. This will not be the case during the evolution of the system, so that the data shown in the above-mentioned figure do not necessarily indicate the evolution of the physical system. The present calculations do not involve simplifications of this kind.

Our task is therefore to verify the numerical method of solving the mean field equations by comparison with Herring's solution and then to extend the study to the evolution of the mean fields, comparing our predictions where possible with a two-dimensional simulation.

The problem is formulated in §2; numerical results which are presented in §§3–5, are compared with the two-dimensional simulation in §6.

The emphasis in this paper is on the broadest features of the time development. In essence we wish to know which features of the time development are retained in the one-dimensional model and to what extent the model time scale is reliable.

2. Statement of the problem

Consider an isothermal layer of fluid at rest confined between rigid horizontal conducting planes a distance H apart and vertical insulating walls a distance typically L apart. If at time zero the temperature of the lower plane is raised from temperature T_0 to temperature $(T_0 + \Delta T)$ and a little thermal noise of r.m.s. amplitude θ' is present, motion will ultimately ensue. If we choose units of length,

H and time H^2/κ, where κ is the thermal diffusivity of the fluid, the flow is specified by:

$$\left.\begin{aligned} A &= \gamma g \Delta T H^3/\kappa\nu, \text{ Rayleigh number;} \\ l &= L/H, \text{ aspect ratio;} \\ \sigma &= \nu/\kappa, \text{ Prandtl number;} \\ \epsilon &= \theta'/\Delta T, \text{ noise figure;} \end{aligned}\right\} \tag{1}$$

where γ is the coefficient of cubical expansion, g is the acceleration of gravity, and ν is the kinematic viscosity. With the above units, the field equations in dimensionless form can be written in terms of horizontal mean quantities together with a 'fluctuating' component (Herring 1963), measuring in a Cartesian frame x, y horizontally and z vertically upwards:

$$\frac{\partial T}{\partial t} = T_{zz} - (\overline{w\theta})_z, \tag{2a}$$

$$\frac{\partial \theta}{\partial t} - \nabla^2\theta + wT_z = \mathscr{M}, \tag{2b}$$

$$\left(\frac{\partial}{\partial t} - \sigma\nabla^2\right)\phi - \sigma A \nabla_1^2 \theta = -\frac{\partial}{\partial x}\mathscr{L}, \tag{2c}$$

$$\nabla^2 w = \phi, \tag{2d}$$

where: (i) (2a) and (2b) represent the decomposed energy equation with the total temperature written as $T(z,t) + \theta(x,y,z,t)$ such that the horizontal mean $\overline{\theta} = (1/l^2)\int\int \theta\, dx\, dy = 0$; (ii) (2$c$) and (2$d$) are derived from the momentum equation, w being the vertical velocity and $\nabla_1^2 = (\partial^2/\partial x^2 + \partial^2/\partial y^2)$ is the 'horizontal' Laplacian; (iii) the terms $\mathscr{M}$, $\mathscr{L}$ represent the fluctuating self-interactions arising from the advection of heat and momentum of the fluctuations acting on themselves.

Before proceeding, it is of interest to see if by a suitable choice of time and length scale the equations could be simplified. The result which follows seems to have been overlooked in the discussions of Herring's work. If we change the length, time and velocity units to δ, δ^2, δ^{-1}, equations (2) remain unchanged except that A becomes $A\delta^3$ and the right-hand side of (2c) is multiplied by $1/\delta$. Hence, provided the source term on the right-hand side of (2c) is negligible, we can rescale the equations and obtain a single solution valid for nearly all A. We can choose δ so that

$$A\delta^3 = A_c = \text{const.} \tag{3}$$

provided $\delta \ll 1$ so that the two sublayers are separated. Now it is known (e.g. Elder 1966*b*, figure 12) that if $\sigma \gtrsim 1$ convective flows behave as if $\sigma = \infty$, when the right-hand side of (2c) is negligible. If, however, $\sigma \ll 1$ we cannot discard this term on these grounds. Here we only consider $\sigma \gtrsim 1$. Hence we solve (2) for one value of A and can immediately obtain solutions at other values of A by means of (3) and the above units. This deduction provides a nice check on the results. We

see from Herring's data (e.g. 1963, p. 336, figure 16) that over the range of Rayleigh numbers $4 \times 10^3 - 10^6$ the results are consistent with the deduction.† We would perhaps have expected, as δ approaches unity (from below), because the two sublayers begin to overlap, that the results would depart from the above correlation. But even at $A = 4 \times 10^3$ with $\delta \approx \frac{1}{6}$ the correlation holds.

It is, nevertheless, necessary to remind ourselves that the above correlations *must* apply if the model is to apply to actual thermal turbulence. In the laboratory the scaling implied by (3) has been confirmed by many workers for thermal turbulence when $\sigma \gtrsim 1$ (e.g. Malkus 1954; Townsend 1959). Hence, strictly the argument must run: given the laboratory data, what simplifications of the field equations lead to the above correlations?

Here we retain the equations in the form (2), since it is easier to relate the solutions to one's previous experience. We shall choose the particular typical Rayleigh number on grounds of convenience. A value of 10^5 is a good choice for experimental work since the flow is turbulent, provided the thermal noise is sufficiently strong, and also for the numerical simulation since δ is not too small to require a prohibitive number of points adequately to represent the fields spatially.

We obtain approximate solutions to (2) after the following simplifications. First, we set the terms $\mathscr{M}$, $\mathscr{L}$ of (2*b*), (2*c*) to zero, the weak coupling approximation. This is not as harsh as it seems at first sight. If $\sigma \gtrsim 1$ the $\mathscr{L}$ term will already be negligible. Further, the structure of the mean temperature field, as determined in the laboratory, reveals thin thermal sublayers dominated by molecular diffusion and a nearly isothermal core. In other words, the mean temperature gradients are only large near the horizontal boundaries and the mean temperature change across the bulk of the flow is so small that a very crude representation of the non-linear fluctuating heat advection, even putting it to zero, cannot effect the essential features of the flow. The vital physical process of molecular diffusion is retained in both (2*a*) and (2*b*) in the $(\partial^2/\partial z^2)$ terms. The second simplification is much more difficult to justify, it is in effect no more than an expedient to reduce (2) from three dimensions to one. We simply write $\nabla_1^2 = -k^2$. That is to say we consider, as does Herring, that there is a single dominant horizontal wave-number, k. There is a further consequence of this reduction, namely we have a problem in one space dimension, z with a velocity $w(z)$ even though the fluid is (nearly) incompressible. Whether or not we can identify k and w with physical elements of actual flows remains to be seen. For the moment they are phenomenological artifacts of this one-dimensional representation. The third, and final, simplification is to replace $\overline{w\theta}$ by $w\theta$. In view of the above comment relating to w this is now a relatively harmless approximation. Also there is some physical validity in the replacement since, as is known from experiment, the major heat transfer mechanism outside the sublayer is the ejection of blobs of sublayer fluid so that w, θ should be strongly correlated. The reader unfamiliar with the ruthless approximations needed to cope with turbulence studies may be surprised that the approximation works at all.

† In particular the Nusselt number $N \propto A^{\frac{1}{3}}$ and the horizontal wave-number for maximum N for given A satisfies $\kappa \propto A^{\frac{1}{3}}$.

With the above simplifications (2) becomes

$$\frac{\partial T}{\partial t} = T_{zz} - (w\theta)_z, \tag{4a}$$

$$\frac{\partial \theta}{\partial t} = \left(\frac{\partial^2}{\partial z^2} - k^2\right)\theta - wT_z, \tag{4b}$$

$$\frac{\partial \phi}{\partial t} = \sigma\left(\frac{\partial^2}{\partial z^2} - k^2\right)\phi - \sigma A k^2 \theta, \tag{4c}$$

$$\left(\frac{\partial^2}{\partial z^2} - k^2\right) w = \phi. \tag{4d}$$

The boundary conditions are: (i) on $z = 0$, $T = 1$, $\theta = 0$, $\phi = 0$, $w = 0$, $w_z = 0$; (ii) on $z = 1, T = 0, \theta = 0, \phi = 0, w = 0, w_z = 0$. The initial conditions are: $T = \frac{1}{2}$, $\phi = 0$, $w = 0$ and a white noise θ field of r.m.s. amplitude ϵ, with $T = 1, 0$ on $z = 0$, 1 at $t \geqslant 0$ except when stated to the contrary. In view of the somewhat arbitrary choice of k we shall use values suggested by Herring's data. These values are near those which lead to a maximum heat transfer for a given Rayleigh number. For example, at $A = 10^5$ we choose $k^2 = 25$. Further, all the present calculations are restricted to $\sigma = 1$.

The above equations are quite similar to the convection equations in two dimensions and represent processes of diffusion, momentum generation from buoyancy forces, but a greatly simplified form representing the advection of heat. Nevertheless, the two essential advective processes are present; heat transports produced by vertical velocity fluctuations working on both temperature fluctuations and on the mean temperature gradient. In particular (4) adequately defines a Bénard–Rayleigh problem, namely for A less than a critical value no persistent motion is possible and $T \to (1 - z)$. There is a further important common feature, namely, if the initial state has zero fluctuation fields θ, ϕ, ω and the boundary conditions are steady the fluctuation fields remain zero. For example, if at $t = 0$: $w = 0$ and hence from (4*d*) $\phi = 0$; from (4*b*) θ remains zero; and hence from (4*c*) ϕ remains zero. For our present task therefore random initial values (generally somewhat less than 1 % of the expected final values) are set as initial conditions for θ, ϕ, w.

The model system (4) involves two phenomenological parameters, k^2 and the ratio $r \equiv (w\theta)/(\overline{w\theta})$. As shown by Herring the solutions are insensitive to the choice of k^2 provided k^2 is chosen near the value for which the Nusselt number N satisfies $\partial N/\partial k = 0$. It is necessary to know also to what extent the solutions depend on r, which throughout this paper will be taken to be unity. It is clear, by inspection of (4) that the coefficient r can be 'removed' from the field equations (and the boundary conditions) by the transformation $(\theta, w, \phi) \Rightarrow (\theta, w, \phi)\sqrt{r}$. Under this transformation the time scale of the motion and the form of T, θ, w, ϕ is unaltered. Only the amplitudes of the fluctuations are altered in the ratio $\sqrt{r}$. Thus if we find later that other considerations require $r \neq 1$ the solutions for θ, w, ϕ can be simply scaled in proportion.

It is important to note that in this model k^2 is a free parameter. We cannot therefore expect the results from this model to apply to actual flows near the

critical Rayleigh number where we know from linear stability theory that at the onset of motion k^2 is determined. The correlations implied by (3) would then no longer apply. Only for sufficiently large Rayleigh numbers, for a given thermal boundary noise, when k^2 is independent of the layer depth could the results of the model provide a representation of actual flows.

The method of solution of (4) is an iterative finite difference technique, using the same methods as I have used before (Elder 1966*b*) apart from the trivial coding changes required for one space dimension rather than two. The outer iteration is organized as the equations are written in (4). Most of the calculations used 100 mesh points and give a precision of better than 0·01 %. Compared to the labour of a simulation in two dimensions a system of equations such as (4) is very straightforward.

Since we have two overlapping requirements, namely to compare Herring's and our results for the steady state and to compare with the two-dimensional simulation it is convenient to consider the two cases of the initial ambient temperature: (i) the symmetrical case of $T = 0{\cdot}5$; (ii) the asymmetric case $T = 0$. The following §§ 3 and 4 treat only case (i), while §§ 5 and 6 treat case (ii). Note that with initial $T = 0$ we have a layer suddenly heated from below, but otherwise we have both sudden heating from below and equal cooling from above.

3. The steady state

Figures 1 and 2 show data† for fully developed solutions of (4) for $A = 10^4$, 10^5 (with $\sigma = 1$). They are very similar to the data given by Herring (1964, p. 282, figures 3–6), with $\sigma = \infty$. This is seen more clearly in the comparison of table 1. Any differences in the data of this table reflect differences solely in numerical technique, largely differences in spatial representation and solution time t. The solution times are more than adequate for convergence to the steady solution, for example, the run here at $A = 10^5$ shows variations about the temporal mean Nusselt number of less than $1:10^4$ at $t = 0{\cdot}1$, but solutions were continued to $t = 0{\cdot}2$. We conclude that the differences are due to the spatial representation. The main weakness in the present representation arises from the term $(w\theta)_z$ in (4*a*) which has the alternative finite difference, far product form $(w\theta_z + \theta w_z)$. Both forms have been used here with negligible (i.e. $< 10^{-4}$) difference in the solutions. Nevertheless, apart from the largest difference in N at 10^5, the differences are very minor when it is clear on other grounds (see § 6) that the model can at best be accurate to perhaps $\pm 10\,\%$.

The profile data for $A = 10^5$ is presented in more detail in table 2. This should be valuable for comparison with other work.

I should like to comment in passing on a few features of this data. (i) One of the intriguing features of the mean temperature profiles obtained both here and in Herring's work is the small bumps on the mean temperature profiles. Figure 3 shows this structure in more detail than can be seen in figures 1 and 2. The magni-

† Note that steady solutions are independent of σ.

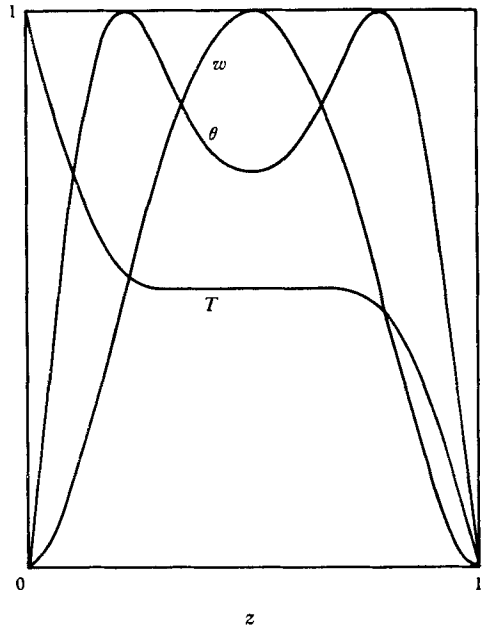

FIGURE 1. Steady profiles of T, θ, w, at $A = 10^4$, $k^2 = 9$. θ-scale = 0·185; w-scale = 21·9.

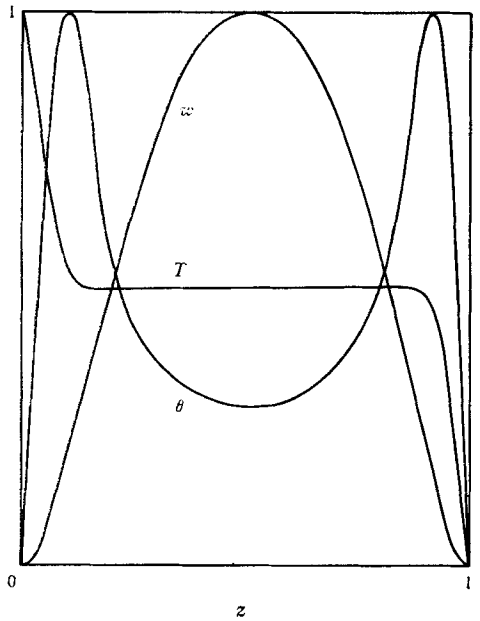

FIGURE 2. Steady profiles of T, θ, w, at $A = 10^5$, $k^2 = 25$. θ-scale = 0·180; w-scale = 123.

R	k^2	w_{max}	θ_{max}	N
4×10^3	9	10·38	0·188	1·989 (1·968)
10^4	9	21·912 (21·95)	0·1847 (0·185)	2·823 (2·824)
10^4	16	24·72	0·183	2·925
10^5	25	122·62 (127·5)	0·1798 (0·20)	6·283 (6·712)

TABLE 1. Data from steady state solutions. In brackets Herring's (1964) data

Unit	0·1798	122·6	1·000
z	θ	w	T
0·00	0·000	0·0000	1·000
0·05	0·7355	0·0639	0·7001
0·10	0·9974	0·2060	0·5234
0·15	0·7644	0·3728	0·4926
0·20	0·5380	0·5347	0·4979
0·25	0·4206	0·6773	0·5004
0·30	0·3574	0·7949	0·5009
0·35	0·3206	0·8856	0·5008
0·40	0·2990	0·9495	0·5006
0·45	0·2875	0·9874	0·5003
0·50	0·2838	1·0000	0·5000

TABLE 2. Normalized steady profile values at $A = 10^5$

tude of the bumps is only about 0·007, and is about half of that seen in Herring's data. I doubt the physical reality of the bump. In my own investigations (Elder 1966*a*) where I have very carefully looked for it, a bump of 0·002 would have been identified. We must not expect too much from the model and an error of form of only 0·7 % should not be taken seriously. (ii) A more disturbing feature of the form of the results is that of θ and w. The laboratory experiments indicate that the interior of the flow has an approximately homogeneous fluctuation field. Certainly the θ, w and $w\theta$ correlations and spectra (Elder 1966*a*; Deardroff & Willis 1967) are independent of position outside the sublayers. In a model of this kind therefore, it would be preferable to obtain θ, w profiles which are nearly independent of z outside the sublayers. The θ field is acceptably constant but the w field is not, the w field retains the $\sin^2 \pi z$ type of form regardless of the Rayleigh number. Any possibility of removing this feature would seem to be the most profitable line to follow in improving this model.

The final approach to the steady state

We observe that the approach to the steady state involves a damped oscillation. This is seen clearly in the data of figure 4 which plots $\log |(N - N_\infty)/N_\infty|$ against t. After the first two cycles the period is nearly constant (e.g. after $t \approx 0{\cdot}3$, the period is about 0·02 for $A = 10^5$, $\sigma = 1$).

The sensitivity of the steady state to small variations in either initial or boundary conditions is a matter of importance. The final solutions found here are not dependent on the initial conditions, provided θ, ϕ, ω are not identically zero. This has been confirmed by a number of solutions with extreme choices of

initial conditions. Further, it is clear from the discussion immediately above that the system will respond to low frequency noise at the boundaries as a highly damped system. Finally, therefore it remains to check the sensitivity of the system to high frequency thermal noise at the boundary. The solutions show that the system is very strongly damped. For example, with random thermal noise of amplitude 0·1 the effects on the mean fields were less than 1 %. Clearly the wall layer acts as an efficient low pass filter.

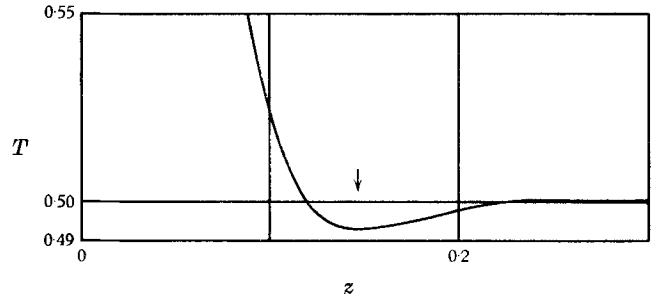

FIGURE 3. Profile detail: $T(z)$ from figure 2.

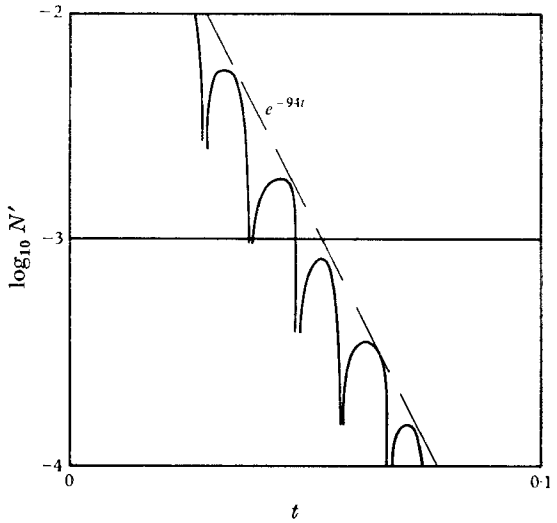

FIGURE 4. Approach to the steady state; relative Nusselt number departure as a function of time.

This behaviour emphasizes an essential difference between this model and laboratory realizations. In the laboratory the wall layer is in a state of continuous instability, with sporadic but persistent production of buoyant elements. This property of continuous instability is not a feature of the present model.

4. The time development: symmetric case

Data showing the development of the fluctuation fields are shown in figure 5. We recognize three distinct phases of the motion: (i) there is an interval, $0 < t < t_1$ during which molecular processes are completely dominant, the advection of heat being negligible. In figure 5, $t_1 \approx 2 \times 10^{-3}$ and is so short that this interval is

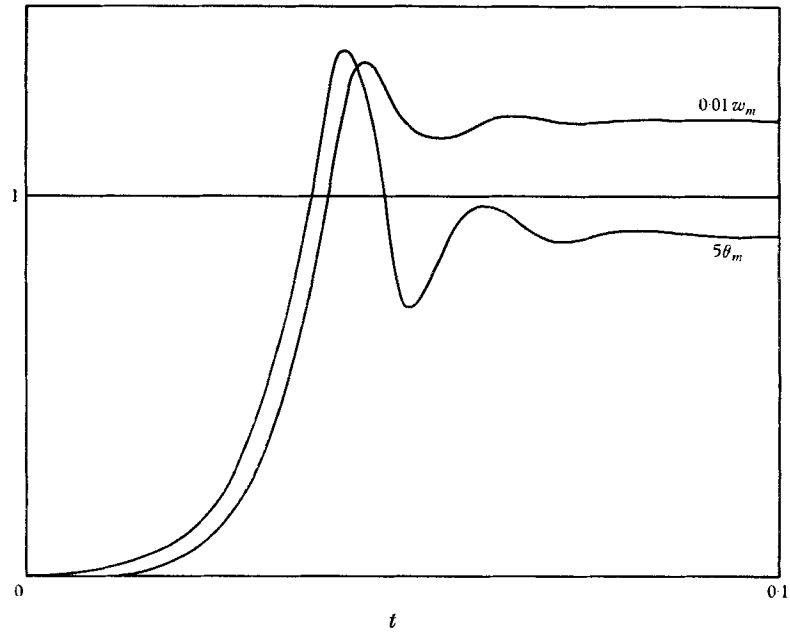

FIGURE 5. Time development of the fluctuation fields θ, w; spatial maxima $\theta_m(t)$, $w_m(t)$: $A = 10^5$, $k^2 = 25$, $\epsilon = 0{\cdot}0087$.

poorly represented. During this interval the system behaves like a thermally conducting solid; (ii) for $t > t_1$ there follows an interval of roughly exponential growth of the fluctuation fields during which the contribution of the non-linear terms becomes increasingly dominant. Towards the end of this interval the non-linear terms are sufficiently large to limit the fluctuation amplitudes to finite values; (iii) in the subsequent time the system behaves like a damped oscillator in the manner referred to in §3 above.

The initial development of the fluctuation fields is seen in the detail of figure 6 which shows $\theta_m(t)$, the spatial maximum value of θ, to be very closely exponential (a more detailed discussion will be given in §6). There is an important consequence of this type of temporal development with a nearly constant growth rate. The time for the fluctuations to grow to finite amplitude is directly related to the initial noise level. For example, if the growth rate $n \equiv \partial \log \theta / \partial t$ and θ_f is the value of θ at which the non-linear processes first begin to limit the exponential growth of the fluctuations ($\theta_f \approx 0{\cdot}15$ for the data of figure 6) the time required is of order $n^{-1} \log (\theta_f/\epsilon)$. The net effect on the subsequent development will be simply a displacement in time of this order. We confirm this idea with the data of figure 7

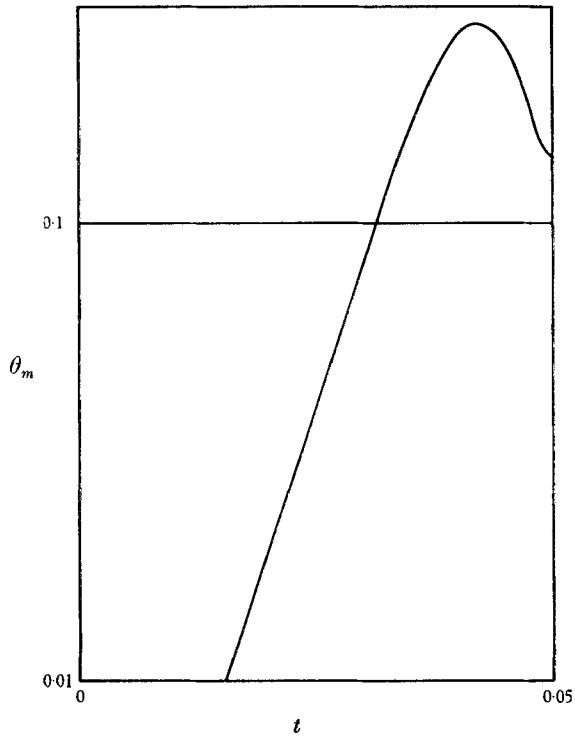

FIGURE 6. Log-linear detail of time development of θ; spatial maximum $\theta_m(t)$; as in figure 5.

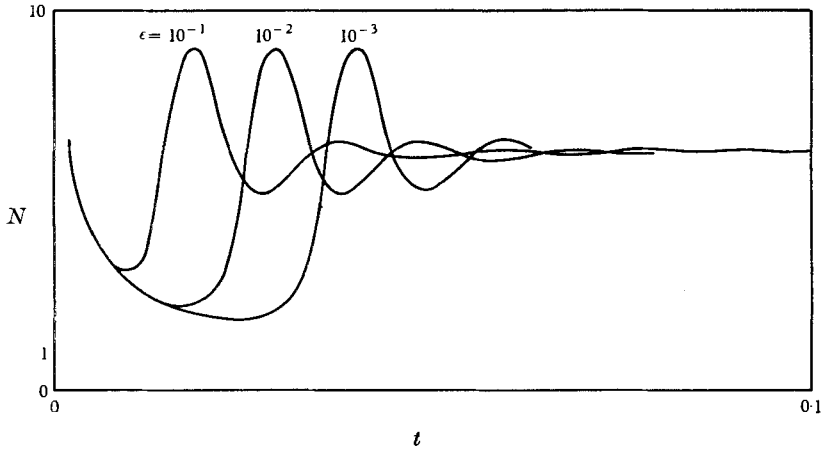

FIGURE 7. Time displacement effect: Nusselt number N as a function of time for three values ϵ of initial thermal noise.

which shows $N(t)$ for various values of ϵ. This observation has an obvious importance when we try to compare our numerical and laboratory results. In the laboratory the very small initial thermal noise levels are difficult to measure reliably so that there is an uncertain time displacement to be kept in mind. Similar considerations will be required when comparing alternative numerical simulations.

The data of figure 5 compares moderately well with somewhat similar data given by Herring (1963, p. 329, figure 1). The time scaling is rather different, but as mentioned above, that is an expected possibility.

The development of the mean profiles is shown in figure 8. During interval (i) the profiles closely approximate the solutions when the T, θ fields are uncoupled from the ϕ, w fields. During interval (ii) θ, w are largely confined to regions near the walls and thereafter in (iii) we approach the steady state. Note at $t = 0{\cdot}04$ the pronounced negative temperature gradient in the central region. This is a reflexion of the tendency in the laboratory for the motion to be dominated by hot blobs rising from the lower boundary and cold blobs falling from the upper boundary.

One of the features of the mean temperature profile of thermal turbulence which has excited considerable interest is the possibility of a similarity form for part of the profile. The existence of such a structure in the lower atmospheric boundary layer has been rather clearly identified by Priestley (1954) and others but identification in the laboratory has not been very successful. Townsend (1959) found little evidence for it in his data, however, Elder (1965, 1966*a*) claims to have found that if such a relationship exists it can only be identified in the 'mixing' region between the conduction dominated wall region and the flow interior. This point of view is also borne out by the recent measurements of Deardorff & Willis (1967*b*). It is of interest to see if there is any evidence for such a region in the present data. Figure 9 presents in log-log form the mean temperature profile as a departure from the central value for $t = 0{\cdot}04$ at $A = 10^5$. The steady-state profile within the wall region, has a monotonically changing slope and therefore cannot be described by a similarity form. But the data at $t = 0{\cdot}04$ does have a rather short straight portion of slope $-\frac{1}{3}$ adjoining the outer portion of the conduction dominated wall region. The fit is about as good as that of laboratory data. At first sight one is tempted to dismiss this observation as barely significant, but the region is in the right place and has the expected slope. It is features of this kind which suggest to this experimenter that the model is along the right lines and worthy of further investigation.

5. The time development: asymmetric case

So far we have presented results for the 'symmetrical' case of simultaneous sudden heating from below and cooling from above. For a simple experimental test this case is rather restrictive since the mean temperature throughout the bulk of the layer remains unchanged. However, in the 'asymmetrical' case of only sudden heating from below there is a development of the mean temperature everywhere in the layer and therefore if we, for example, measure $T(\frac{1}{2}, t)$, which

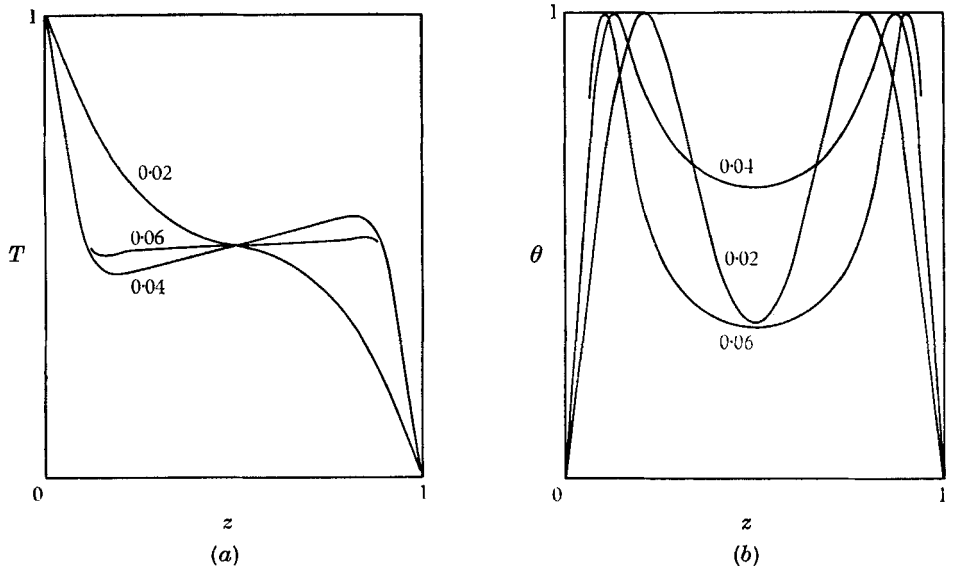

FIGURE 8. Symmetric case profiles at $t = 0{\cdot}02, 0{\cdot}04, 0{\cdot}06$; $A = 10^5$, $k^2 = 25$, $\epsilon = 0{\cdot}0087$: (*a*) T; (*b*) θ, scales 0·020, 0·255, 0·200. The w-profiles are similar to those in figure 2 but with scales: 5·18, 118, 123.

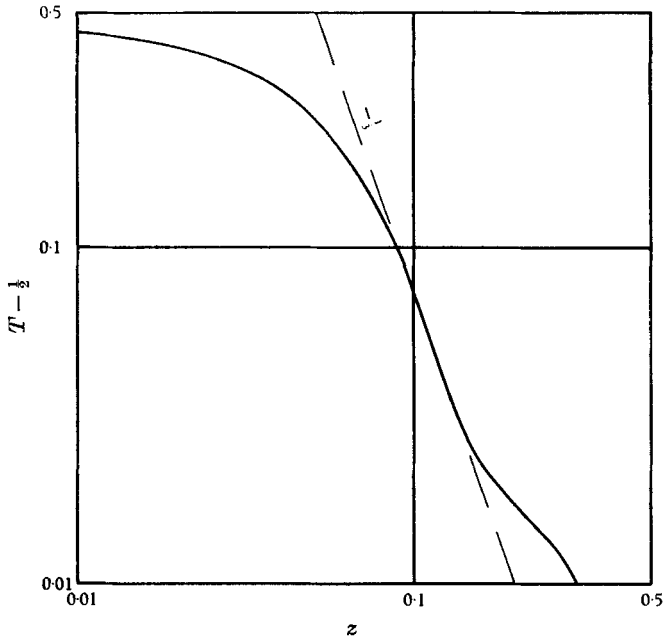

FIGURE 9. Log-log detail of $T(z)$ at $t = 0{\cdot}04$ as in figure 8(*a*).

is straightforward, we could compare the evolution of the model and the experiment. In addition this is the type of situation of interest where one might wish to use the weak coupling approximation in evolutionary studies. The most important feature of the asymmetrical case in the present context is that the system exhibits two distinct time scales: the time scale of the sublayer and the time scale of accumulation of thermal energy in the layer as a whole, in other words the time of heating up. The symmetrical case exhibits only the former time scale. Now the average temperature of the whole layer, T_m, clearly satisfies $\dot{T}_m = N_0 - N_1$ where N_0 and N_1 are the Nusselt numbers for $z = 0$ and 1 so that the time scale (of T_m) is proportional to $A^{-\frac{1}{3}}$, as expected from dimensional analysis. But since both N_0 and N_1 involve t in a different manner the constant of proportionality will be different from that of the sublayer.

Figure 10 presents data showing the development of the mean profiles for the asymmetrical case. Many of the features of the profiles are the same as those seen above and need no further comment, but the form of the mean temperature profile is unexpected. The motion for $t < 0{\cdot}02$ is largely independent of conditions near the upper boundary. Such an interval is expected, but during this time the mean temperature profile develops a pronounced bump corresponding to initial eruption of blobs from the protosublayer. In the laboratory and in the two-dimensional simulation, entrainment and almost complete separation of the rising blob from the sublayer are essential features of the initial destruction of the protosublayer. Neither of these processes can be represented by a one-dimensional model, yet the gross features of the eruption of the buoyant elements are.

6. Comparison with the two-dimensional simulation

We now compare the behaviour found in this one-dimensional model with that found in the two-dimensional simulation of the protosublayer (Elder 1968*a*). Much of the detail is necessarily lost but the broad features remain. The development of the profiles during interval (ii) is particularly interesting since it corresponds to the period of vigorous convection in the protosublayer prior to and during the eruption of the buoyant elements.

The development of the flow in two dimensions† is represented in the field distributions of figure 11. The field distributions show the eddies embedded in the protosublayer till time 0·02, the period of eruption of the buoyant elements at $t \approx 0{\cdot}03$ and the subsequent domination of the flow by the large-scale eddying motions in the interior.

The final growth rate n given by the data of figure 10 can be compared with the final growth rates estimated during the corresponding two-dimensional simulation of the protosublayer (Elder 1968*a*, table 1). These data are compared in figure 12. The data lie near the same line $n \propto A^{\frac{2}{3}}$, which is expected from dimensional analysis as indicated in the discussion of scaling in §2.

The above discussion overlooks two features of the initial development: the

† Data has been taken from the solutions obtained by Elder (1968*a*), but where necessary further solutions have been found by identical methods.

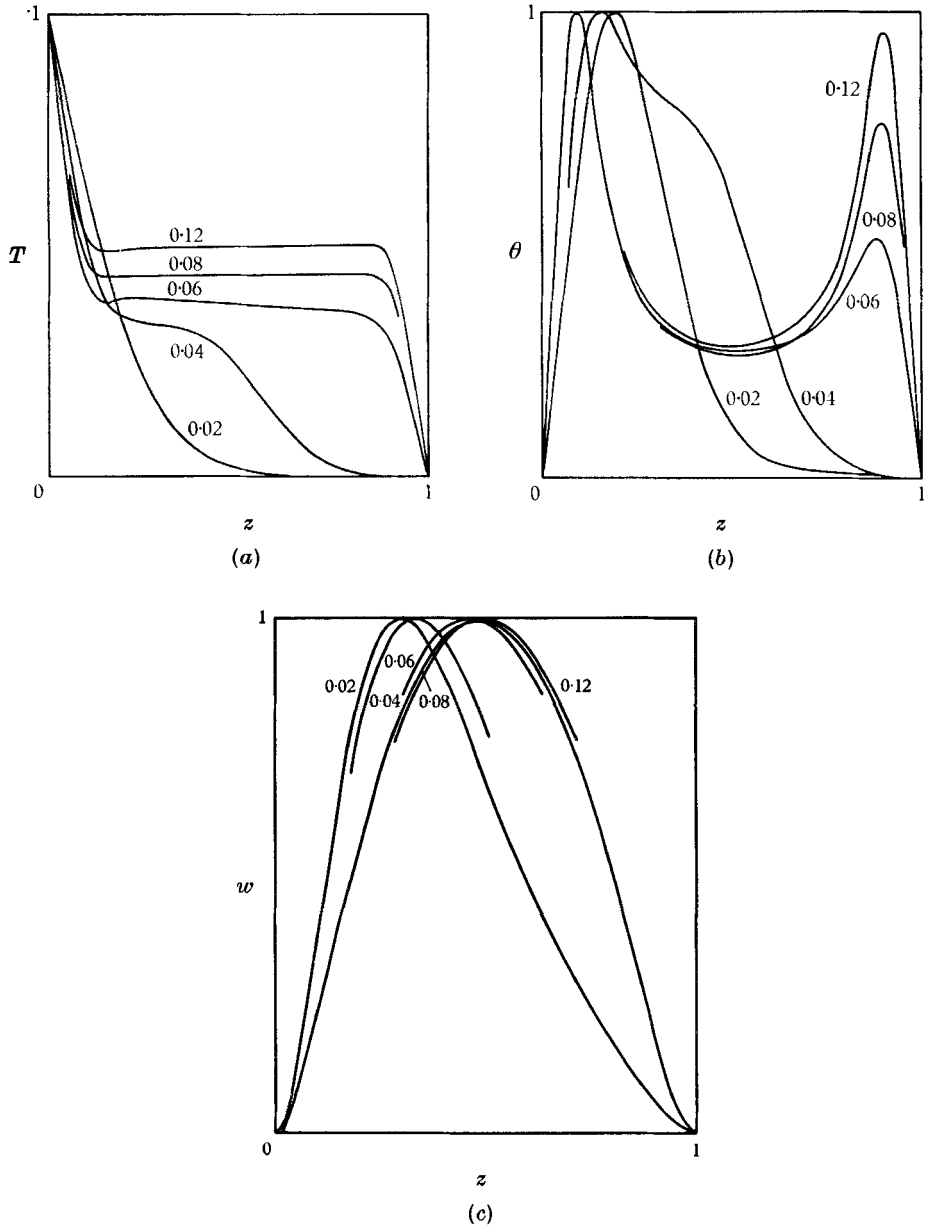

FIGURE 10. Asymmetric case profiles at $t = 0{\cdot}02$–$0{\cdot}12$; $A = 10^5$, $k^2 = 25$, $\epsilon = 0{\cdot}0002$: (*a*) T; (*b*) θ, scales 0·007, 0·288, 0·215, 0·202, 0·189, 0·185; (*c*) w, scales 0·99, 64·7, 118, 122, 123, 123.

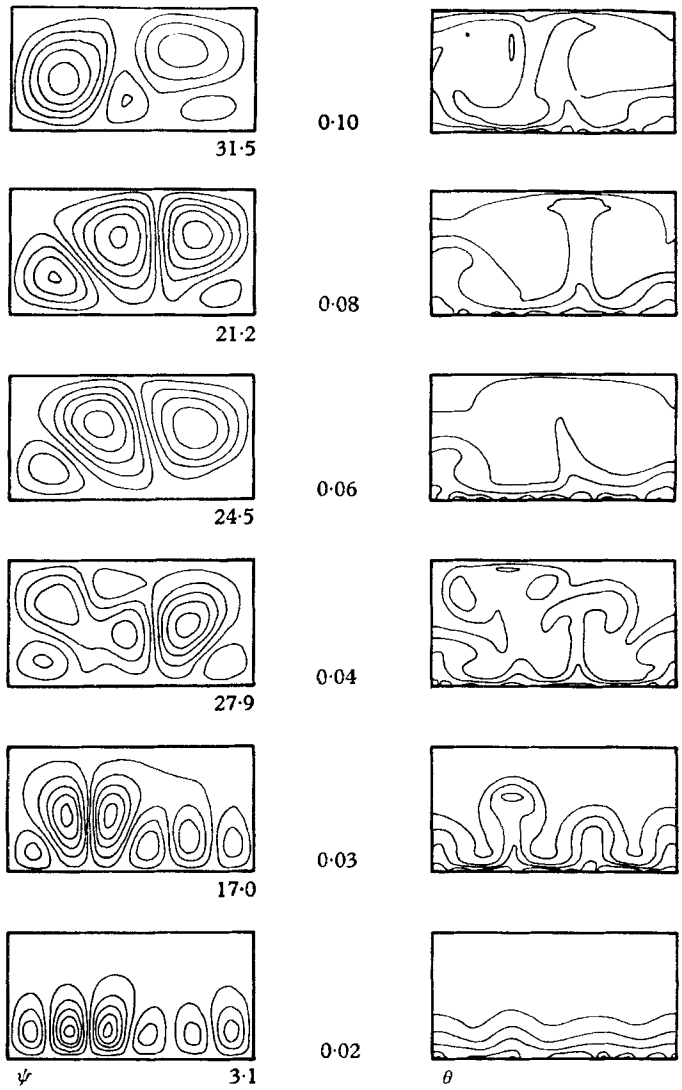

FIGURE 11. Field distribution of stream function ψ and temperature θ at $A = 10^5$, $\sigma = 1$, $l = 2$: two-dimensional simulation.

finite critical time and the non-constancy of the growth rate. These features are obscured in the data of figure 6, where the time resolution is rather coarse. But the data of figure 13 with both a lower initial thermal noise and finer time resolution clearly shows the critical time and the non-constant growth rate. By repeating the calculation for various ϵ I have verified that apart from a change of level the shape of the curve in figure 12 is independent of ϵ provided ϵ is sufficiently

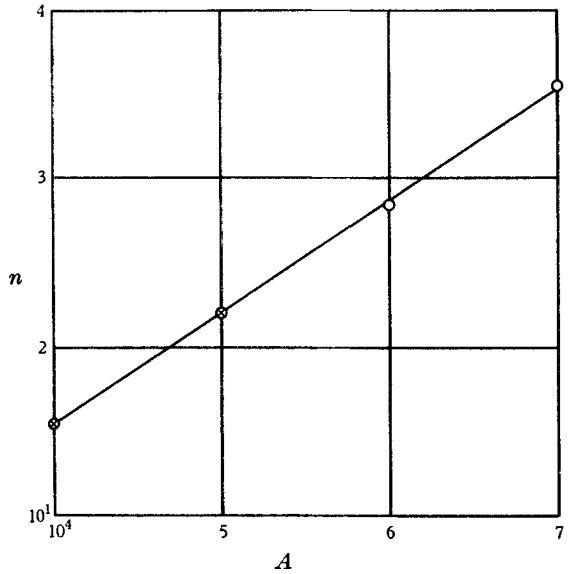

FIGURE 12. Comparison of growth rates $n(A)$ for one- ⊗ and two-dimensional ○ simulations, asymmetric case: $A = 10^5$, $k^2 = 25$.

small. In particular the critical time, at which amplification begins, is independent of ϵ. At $A = 10^5$ the critical time is $2{\cdot}65 \times 10^{-3}$. If, however, $\epsilon \geqslant 10^{-2}$ (at $A = 10^5$) the critical time and the superexponential region are amplitude dependent. This is because the imposed temperature fluctuations are 'finite' and the non-linear terms in (4) are important from time zero. The growth rate itself is shown in figure 14. These data are qualitatively similar to those obtained in the two-dimensional simulation. The superexponential and exponential regions are seen in both sets of data. The form of $n(t)$ seen in figure 14 is however different in detail from that suggested in Elder (1968*a*, equation (20)).

In this connexion the data of figure 10 highlight a feature of the profiles we have so far overlooked, namely that the thickness of the thermal sublayer passes through a maximum and is then reduced because of the increasing vigour of the interior motion. This observation aids the interpretation of the data of figure 14. In the heuristic analysis of Elder (1968*a*) it was assumed that throughout the interval of 'exponential' growth the protosublayer thickness was monotonically increasing proportional to $\sqrt{t}$. Whence it follows that n should monotonically decrease; although increasingly slowly. But as seen in figure 14, after a time, n becomes very nearly constant. Hence the final phase of nearly exponential growth is achieved through active modification of the mean temperature profile,

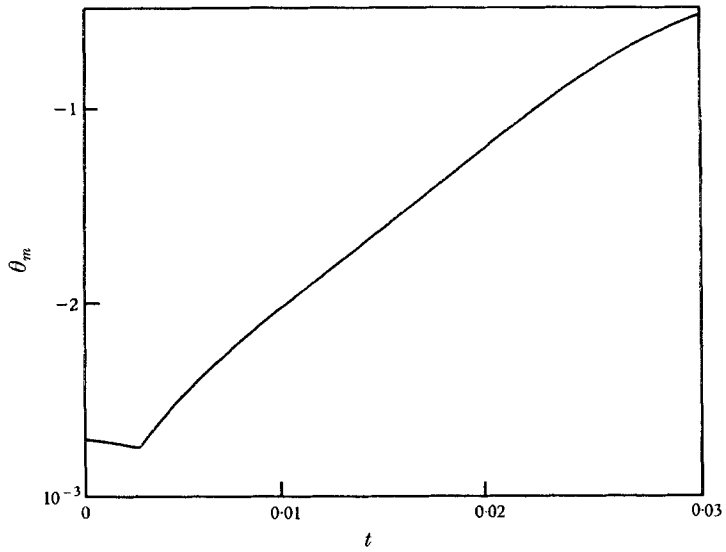

FIGURE 13. Log-linear detail of $\theta_m(t)$, showing critical time and superexponential region, asymmetric case, $A = 10^5$, $k^2 = 25$.

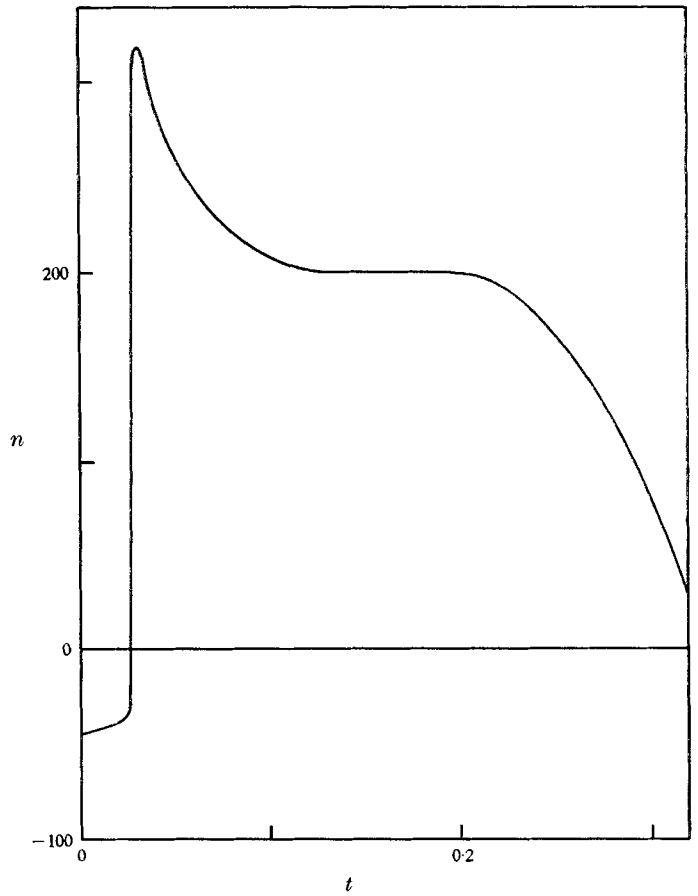

FIGURE 14. Growth rate $n(t)$ for the flow of figure 13.

arising from the finite amplitude fluctuations, rather than because the asymptotic state $t \to \infty$ has been reached. In other words the fluctuations play an important dynamical role earlier than was previously suggested.

The adequacy of the overall development of the flow can be appreciated from the heat transfer data of figure 15. The time scales are quite similar as can be seen from the time of first amplification, the time of the first peak and the time of approach to the final state. The subsequent details are however quite unrelated and the final mean level is roughly 20 % higher for the one-dimensional model.

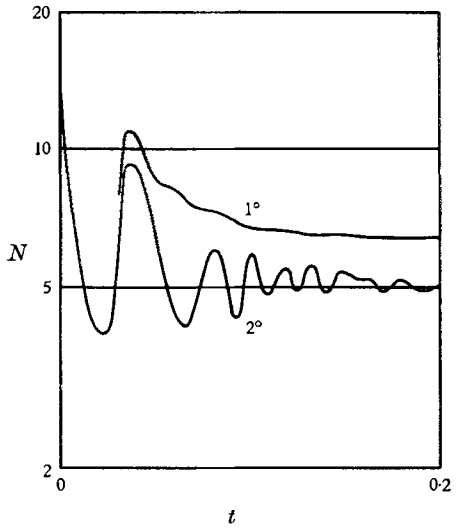

FIGURE 15. Comparison of Nusselt number development for one- and two-dimensional simulations, asymmetric case, $A = 10^5$.

While strictly we must take the model system (4) at face value it is tempting to identify the quantities θ, w, ϕ with corresponding quantities in the two-dimensional simulation. This is a rather suspect procedure since we are really trying to get more from the model than has been put into it. For example, we show in figure 16 the mean profiles for the two-dimensional simulation of T, θ', w' where θ', w' are r.m.s. departures from the horizontal means. These profiles are strikingly similar in form to the profiles of figure 10. The major discrepancy is in the amplitudes of θ' and w'. The ratio $(\theta'/\theta)/(w'/w) \approx 5$, whereas it should be approximately unity. This is disturbing and I am unable to account for it. At the moment if we wished to identify θ with θ' then values of w are about five times higher than w'.

The numerical simulations indicate that the weak coupling approximation provides an adequate description not only of the final (statistically) steady state but of the evolution of the mean fields from a state of rest towards the (statistically) steady state. There are several features of the model however which deserve further investigation. The complete neglect of the fluctuating interactions is not very serious provided $\sigma \gtrsim 1$, but the ad hoc nature of the choice of k is disturbing, when it is clear from experiment that the horizontal wave-number spectrum is very broad.

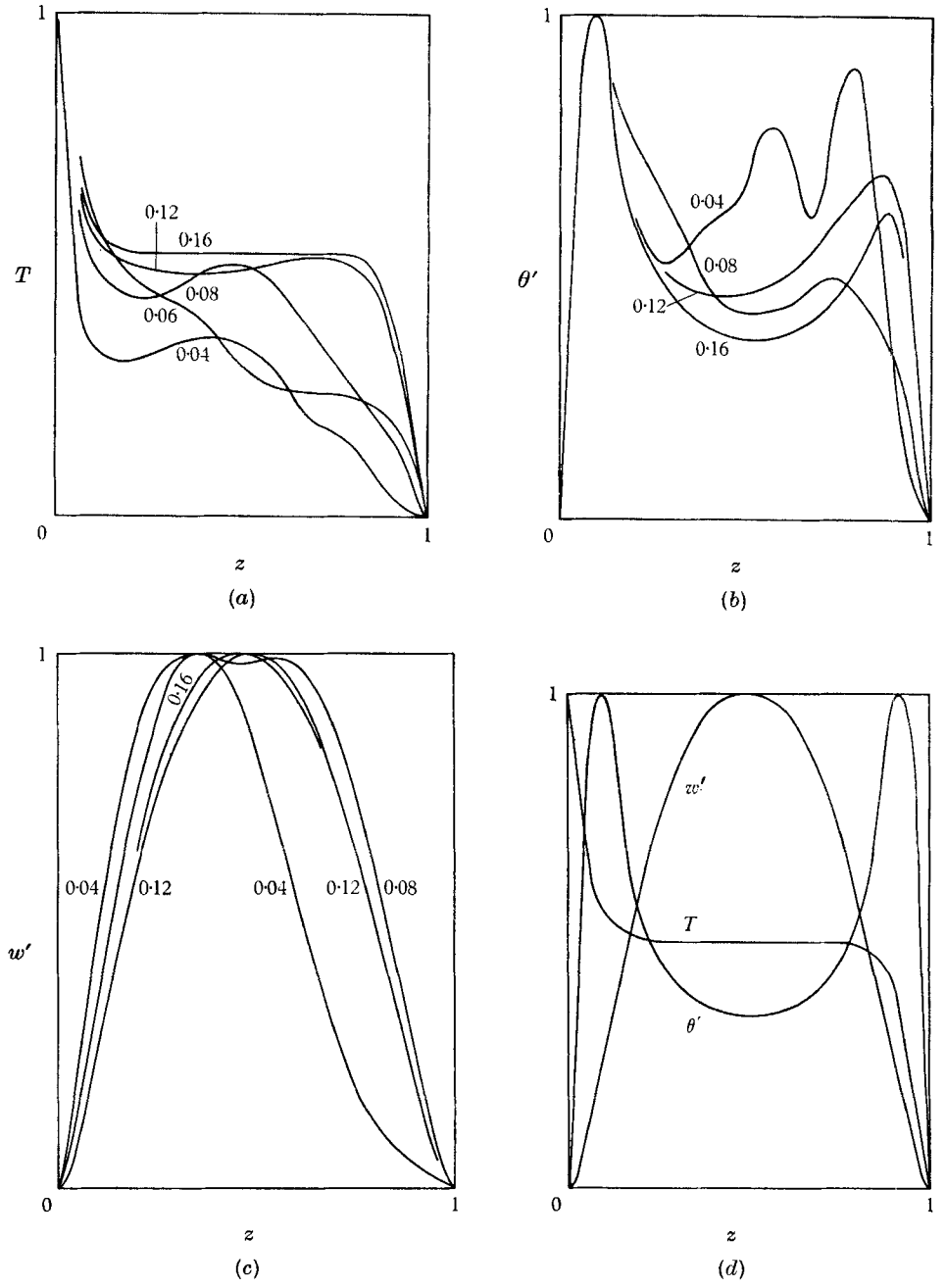

FIGURE 16. Profiles of :(*a*) T; (*b*) θ'; scales 0·203, 0·124, 0·198, 0·183, 0·191; (*c*) w'; scales 8·9, 8·6, 17·6, 22·6, 21·8; at various times corresponding to the flow of figure 11, where θ', w' are r.m.s. departures from horizontal means; (*d*) in the steady state, θ' scale = 0·19; w' scale = 24.

This work was supported by the British Admiralty, The National Environmental Research Council and a grant from IBM (U.K.). The numerical study was performed on the Cambridge Mathematical Laboratory's *Titan*.

REFERENCES

DEARDORF, J. W. & WILLIS, G. E. 1967*a* *J. Fluid Mech.* **28**, 675.
DEARDORFF, J. W. & WILLIS, G. E. 1967*b* *Quart. J. Roy. Met. Soc.* **93**, 166.
ELDER, J. W. 1965 *J. Fluid Mech.* **23**, 99.
ELDER, J. W. 1966*a* Second Australasian Conference on Fluid Mechanics.
ELDER, J. W. 1966*b* *J. Fluid Mech.* **24**, 823.
ELDER, J. W. 1968*a* *J. Fluid Mech.* **32**, 69.
ELDER, J. W. 1968*b* *Sci. Prog. Oxf.* **56**, 1.
HERRING, J. R. 1963 *J. Atmos. Sci.* **20**, 325.
HERRING, J. R. 1964 *J. Atmos. Sci.* **21**, 277.
MALKUS, W. V. R. 1954 *Proc. Roy. Soc.* A **225**, 185.
PRIESTLEY, C. H. B. 1954 *Aust. J. Phys.* **7**, 177.
SPIEGEL, E. A. 1965 *Proc. 5th Cosmical Gas Dynamics Symposium*, Nice.
TOWNSEND, A. A. 1959 *J. Fluid Mech.* **5**, 209.

Note added in proof. The phrase 'evolutionary studies' may not be clear to all readers. Let me give an illustration. For example, a thermal history of the earth can be constructed by considering the cooling of a hot sphere of viscous fluid (Elder 1968*b*, § 6). In spite of its all too obvious weaknesses, the weak-coupling approximation allows for the first-time studies of such models. This is immense value to the geophysicist. Unfortunately, the astrophysicist modelling stars with $\sigma \sim 10^{-9}$ must wait development of suitable representations of the term $\mathscr{L}$ in (2*c*). It is to be hoped that the work begun by Spiegel (1968) and his colleagues with these 'strong-coupling' approximations will soon bear fruit.